Received: 9 October 2023 | Revised: 30 November 2023 | Accepted: 15 December 2023

DOI: 10.1111/jace.19672

Journal of the American Ceramic Society

RESEARCH ARTICLE

Phase purity and evolution in sol–gel derived single component and multicomponent rare-earth disilicates

Alejandro Salanova[1] | **Elizabeth J. Opila**[1] | **Jon F. Ihlefeld**[1,2]

[1]Department of Materials Science and Engineering, University of Virginia, Charlottesville, Virginia, USA

[2]Charles L. Brown Department of Electrical and Computer Engineering, University of Virginia, Charlottesville, Virginia, USA

Correspondence
Alejandro Salanova, Department of Materials Science and Engineering, University of Virginia, Charlottesville, VA 22904 USA.
Email: as2ej@virginia.edu

Funding information
National Science Foundation, Grant/Award Number: 1921973

Abstract

Rare-earth disilicates are a focus of study for use as environmental barrier coatings in gas-turbine engines. These coatings require thermomechanical and thermochemical stability at elevated temperatures and properties can be tailored through the use of multicomponent rare-earth disilicates. Producing rare-earth disilicates via sol–gel is documented in literature, but there are differing procedures with varying phase purities. This work establishes trends that dictate the effects of water content, pH, and heat treatment conditions that determine the final phase purity of Yb, Er, Lu, Sc, and Y disilicate powders made via sol–gel. The phase(s) of the powders were identified and quantified using X-ray diffraction (XRD) to extract weight fractions. In situ XRD during heating from room temperature to 1200°C was used to observe the crystallization and phase evolution of the sol–gel-based powders, allowing for the identification of a rarely reported low temperature triclinic phase in ytterbium-, erbium-, and lutetium-based disilicate sol–gels that forms prior to transformation into a monoclinic phase. Ex situ XRD allowed for the phase identification of sol–gels processed at 1400°C. These experiments demonstrated that phase-pure disilicates could be formed under conditions with no intentional water additions, a target pH of 2, and long heat treatment times at high temperatures (e.g., 1400°C). These conditions remain valid for not only single-cation rare-earth disilicates of Yb, Er, Lu, Sc, and Y but also a multicomponent disilicate containing equimolar concentrations of all of these cations.

KEYWORDS
environmental barrier coatings, phase transition, sol–gel, synthesis, X-ray methods

1 | INTRODUCTION

Thermal and environmental barrier coatings (T/EBCs) are required for protecting silicon carbide-based ceramic matrix composites (CMCs) from deleterious reactions at elevated temperatures in gas turbine combustion environments.[1–11] To adequately protect the underlying CMC, the T/EBC must possess a low coefficient of thermal expansion (CTE) mismatch, phase stability through the application temperature range, a high melting temperature, and reduced silica activity relative to phase-pure silica.[6] One viable candidate material system possessing

these criteria for T/EBC applications is the rare-earth disilicate (REDS). Despite their promise, REDS can still undergo reactions with water vapor and transform into monosilicates (MS) or oxides with distinct properties not always beneficial in T/EBCs. The thermomechanical and thermochemical properties of REDS can be tailored and improved through the inclusion of additional rare-earth cations to produce a multicomponent REDS.[12–14]

Increased numbers of rare-earth cations past a single cation all the way up to high entropy compositions have also been used to modify the macroscopic properties of solids such as thermal expansion and thermal conductivity.[12–15] For multicomponent compositions, rare-earth disilicates benefit from the large number of available rare-earths (the lanthanides as well as scandium and yttrium) that can be incorporated. The choice of which cations are to be included will influence the final material polymorphs due to differences in ionic radii, as reported by Felsche.[16,17] From the many possible compositions/polymorphs to use in applications, the monoclinic phase (sometimes referred to as the Type-C or β phase) that consists of the smallest cations (i.e., Sc, Lu, and Yb) with the $C\,2/m$ space group is the most viable for T/EBC purposes. The $C\,2/m$ phase has a compatible CTE with respect to SiC and has been reported to have no polymorphic transformations upon heating.[14,16,18]

The literature contains many different synthesis techniques for REDS, but one of the most common is the sol–gel method given the many years of foundational work in the synthesis of silicates via sol–gel processes.[14,19–26] Typically, a rare-earth nitrate and tetraethyl orthosilicate (TEOS) are used as a precursors dissolved in an alcohol-containing solution at different pH levels. The resulting powders vary in phase purity from single-phase disilicates to a phase mixture containing the MS phase (e.g., RE_2SiO_5) where the residual SiO_2 may be present as a tertiary amorphous phase. Several prior works understated the presence of the secondary phases due to the extremely low intensity of peaks in X-ray diffraction (XRD) analysis, whereas others attempted to remove the secondary MS phase by adding excess TEOS to react out any silica deficient MS phase.[14,19–21,23–25] The presence of excess silica is deleterious to the performance of a T/EBC, however, given that silica has a melting point several hundred degrees lower than the REDS and a high reactivity with water vapor in combustion environments, requiring its removal before use.[27] When REDS-based T/EBCs see real-world use, they are typically applied through plasma spray deposition. The highly energetic process frequently results in an amorphous coating that upon crystallization can contain varying quantities of mono- and disilicates. As such, knowledge of the progression of phase formation from amorphous-to-crystalline is desired.

TEOS is a metal alkoxide, which typically reacts readily with water. This reaction is known as hydrolysis as a hydroxyl ion becomes attached to the metal atom.[28,29] The reactions for partial and complete hydrolysis of TEOS are shown in Equations (1) and (2), respectively.

$$Si(OR)_4 + H_2O \rightarrow HO - Si(OR)_3 + ROH. \quad (1)$$

$$Si(OR)_4 + 4H_2O \rightarrow Si(OH)_4 + 4ROH. \quad (2)$$

In these reactions, R represents an ethyl group. Understanding the reactions that occur during the REDS sol–gel process can allow for tailoring weight fractions of the various phases of rare-earth silicates or producing a phase-pure REDS. Hydrolysis of TEOS is catalyzed by the presence of H^+ and OH^-, with a minimum in reaction rate in the pH range of 4–7. The rate of the hydrolysis reaction increases with the concentration of H^+ and OH^-species, meaning that pushing pH to high or low extremes promotes the conversion of TEOS to silica.[28,29] Sol–gel synthesis of REDS has also resulted in previously unobserved phases. For example, Zhao et al.[30] reported that a triclinic phase crystallized in Yb disilicate that had otherwise not been seen in literature. This triclinic phase is not present in published phase diagrams or in Felsche's previous reports on the polymorphs of REDS. Other rare-earth cations do have well reported monoclinic and triclinic polymorphs, such as erbium and yttrium disilicate.[16,20] According to Felsche,[16] the triclinic and monoclinic phases of erbium disilicate have the following cell parameters: $a = 6.583$ Å, $b = 6.609$ Å, $c = 12.000$ Å, $\alpha = 94.50°$, $\beta = 90.57°$, and $\gamma = 91.79°$ for the triclinic phase, and $a = 6.841$ Å, $b = 9.135$ Å, $c = 4.694$ Å, and $\beta = 101.70°$ for the monoclinic phase and differing molar volumes for the two phases. The presence of this triclinic phase may complicate the phase stability of the T/EBCs required for thermomechanical stability via phase transformations during the initial heating and crystallization of the plasma-spray deposited coating or even during heating and cooling cycles in normal use.[16,27] The present study focuses on the processing parameters that control the resulting phase of single component and a multicomponent REDS made via sol–gel with a focus on the parameters that enable preparation of phase-pure REDS. In addition, the phase evolution of these REDS from the xerogel to the final crystalline product is studied during heating via in situ XRD.

2 | EXPERIMENTAL METHODS

2.1 | Sol–gel synthesis

Yb, Er, Lu, Sc, Y, and a multicomponent (containing all five cations listed) REDS were synthesized via a sol–gel method

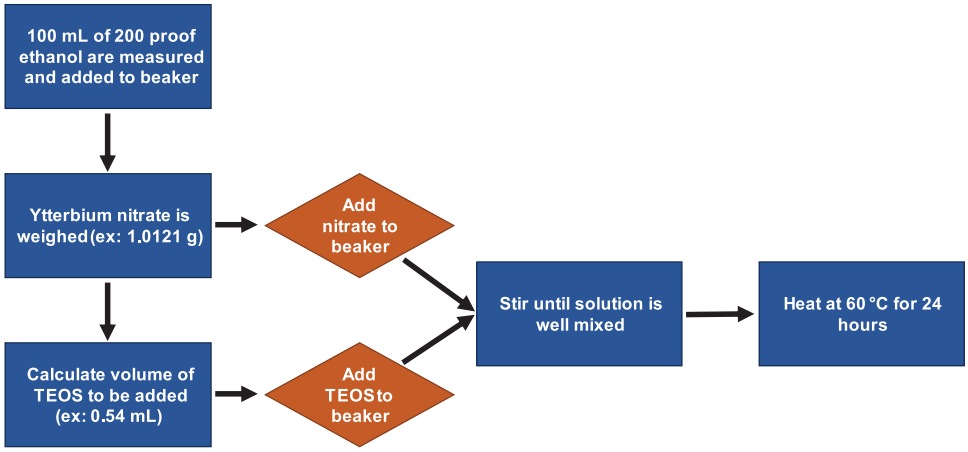

FIGURE 1 Experimental flowchart showing a synthesis procedure of a Yb disilicate sol–gel with the mass and volume for the nitrate and tetraethyl orthosilicate (TEOS) respectively.

with a procedure that was modified from previous work and is depicted via a flowchart in Figure 1.[14] Rare-earth nitrates (99.9% purity, Alfa Aesar) and TEOS (98% purity, Acros Organics) precursors were mixed into a 100 mL reaction solution where the nitrates were weighed and then the corresponding volume of TEOS required was calculated based on molecular weight and density. The volume of TEOS corresponded to a 1:1 molar ratio to the rare-earth cations present. Typical conditions used 2.4×10^{-3} moles of the rare-earth nitrate and TEOS in the 100 mL solution. The water content of the rare-earth nitrates was measured via thermogravimetric analysis (Netzsch STA-449 F1). The water content was accounted for in the composition calculation. The rare-earth nitrates and TEOS were dissolved in a reaction solution to dissociate ions and induce the hydrolysis reactions described in Equations (1) and (2). The rare-earth nitrate ion dissolution is described by Equation (3).

$$RE(NO_3)_3 + H_2O \rightarrow (RE(OH_2))^{3+}_{aq} + 3NO^{-}_{3_{aq}} \quad (3)$$

The reaction solution contained anhydrous ethanol and deionized water. The ratio of the two solvents was varied to determine the effects of water content on phase formation. The pH was then modified as either hydrochloric acid or ammonium hydroxide were added dropwise via a syringe until a desired pH was reached as measured by a pH meter (Fisher Scientific Accumet AE150 pH Benchtop Meter). The reaction solution was stirred until no visible precursor remained, after which the solution was placed on a hot plate that was set to 60°C without stirring. The dissociated rare-earth ions and silica containing organics are presumed to be homogenously distributed through the mixture. The rare-earth ions will form an aqueous rare-earth oxide, whereas the TEOS is hydrolyzed to produce silica.[20] The aqueous silica and rare-earth oxide form a linked network of precipitates as the reaction solution is evaporated during heating. The solution was left to gel, which took varying amounts of time depending on water content (1–3 days with higher water content taking longer). Once the gel formed, it was transferred to a platinum crucible and dried in a box furnace (Thermo Scientific Thermolyne) at 550°C for 24 h in static ambient air to form a xerogel. The resulting xerogel was crushed in a Diamonite mortar and pestle until a fine powder remained. The powder was returned to a platinum crucible and exposed to a 1400°C static ambient air environment for 18 h in a box furnace (Rapid Temperature Furnace, CM, Inc.) to form the crystalline product. For the multicomponent REDS, the same procedure was followed using equimolar quantities of each rare-earth cation added as nitrate precursors, and the appropriate molar quantity of TEOS was added to ensure a RE:Si ratio of one. The first rare-earth cation selected for synthesis was Yb, followed by Er, Y, Lu, Sc, and a multicomponent mixture of all five cations. The fraction of water was varied, ranging from 0, 10, 50, and 90 mL of water out of the total 100 mL reaction solution.

2.2 | Diffraction experiments

Two sets of diffraction experiments were performed using XRD: ex situ (i.e., after heating the powder in a furnace) and in situ (i.e., performing XRD while heating the powder). The reason for both was due to temperature limitations in the in situ heating furnace. The purpose of the in situ heating XRD experiments was to observe the crystallization behavior and phase evolution as the temperature increased. The in situ work had an upper limit of 1200°C. The ex situ experiments measured the room temperature diffraction patterns of the powders after they were heated in a furnace to 1400°C. The ex situ

diffraction experiments were performed with a Malvern Panalytical X'pert X-ray diffractometer (Cu K_α X-ray wavelength of 1.54 Å) to identify and quantify the phase fraction of the REDS powders. A Bragg–Brentano geometry and X'celerator detector were used to perform powder diffraction experiments and the powder was continuously rotated using a spinner stage during the measurement. Once the ex situ XRD experiments identified solvent parameters that resulted in a phase-pure REDS after 1400°C furnace heat treatment, the in situ experiments were conducted. The in situ experiments involved the same synthesis procedure as previously described but the process was stopped after the 550°C box furnace step. After the 550°C xerogel product was ground into a powder, in situ hot stage XRD was performed using a Malvern Panalytical Empyrean X-ray diffractometer (Cu K_α X-ray wavelength of 1.54 Å) in a Bragg–Brentano geometry, an Anton Parr HTK1200N hot stage, and GaliPIX3D detector. The temperature was ramped at a rate of 10°C/min stopping at 50-degree intervals between 50 and 1200°C for approximately 15-min holds to perform XRD scans over a 10°–90° 2θ range.

2.3 | Phase identification

The collected diffraction patterns were analyzed using GSAS-II software to quantify weight fractions of the observed phases.[31] The phases for the rare-earth disilicate, MS, and oxide were imported from crystallography information files (*.CIF) collected from the ICSD database.[32–34] The residual weight percent (R_{wp}) for every refinement of the weight fraction was in the range of 9%–13% for all experiments in this manuscript. Phase identification for hot stage data was performed using HighScore Plus (Malvern Panalytical) software after the patterns were collected.

3 | RESULTS AND DISCUSSION

3.1 | Effect of water content and pH on phase formation

Figure 2 shows the XRD patterns for all the pH of 2 Yb REDS sol–gels. The XRD patterns for the other pH values are provided in Figures S1 and S2. Table 1 shows the phase weight percentage results of the Yb solvent dependence experiments after heat treatment of the powders at 1400°C, where the numbers given correspond to the disilicate monoclinic phase (space group $C\,2/m$). The percentages given in parentheses correspond to the weight percent of MS phase, if there is a MS present. If the balance does not equal 100%, then the percentage is completed by the presence of ytterbium oxide. Starting with the effect of water content for fixed pH ranges, the following observations were made: The solutions containing the most quantities of water did not produce single-phase REDS, instead two or more phases were identified, typically the desired disilicate and the undesired MS, regardless of pH. This is evident in Figure 2 where for a pH of 2 and no intentional water additions, a phase-pure disilicate was prepared. However, for the same pH of 2 with 90% H_2O in the solution, the derived powder had >85 wt.% MS phase. Similar trends were observed for the pH of 10 where the no intentional water content had >97 wt.% disilicate phase, but the 90% water content was primarily MS. The trends also held for intermediate pH values. These are described as "Unaltered" pH in Table 1. The "Unaltered" category had pH values in the range of 4 up to approximately 6, with the lowest values corresponding to the lowest quantities of water. The exact values are given in Figure S2. The pH meter read a value of 4 when measuring the solution with 0% water (all anhydrous ethanol). Here, low water content (0% and 10%) derived powders were primarily composed of disilicate phases. However, increasing the water content to 50% and 90% led to no observable disilicate peaks in XRD and mixtures of MS and rare-earth oxides were observed. The only other condition that led to rare-earth oxide formation was 90% water and a pH of 2. In observing the trends of phases present for fixed water content and varied pH (i.e., vertical columns on Table 1), it is generally observed that the low pH and high pH solutions led to the highest disilicate phase fractions. Using high pH (pH = 10) or low pH (pH = 2) resulted in higher disilicate fractions over those syntheses in which solution pH was not intentionally controlled. The largest content of disilicate phase formation over the broadest range of water content was observed for the low pH condition, followed by the high pH condition. It is hypothesized that solutions at pH of 2 undergo a faster hydrolysis reaction than in the unaltered solutions. The solutions require more H^+ to increase the hydrolysis reaction rate, therefore increasing reaction rate with lower pH values and free sufficient silica from TEOS to produce the disilicate. While at or just below neutral pH values, the unaltered solutions have a comparatively slow rate hydrolysis reaction.

From these data, the observed trend is that little to no water and low pH in the reaction solution is required to achieve a phase-pure disilicate. These results may seem contradictory to the reaction provided in Equation (1), with water being necessary for the hydrolysis of TEOS to occur. However, the water in the TEOS hydrolysis reaction can come from two sources: The rare-earth nitrates that are hygroscopic and are sourced as rare-earth nitrate hydrates, and the other source is humidity in the ambient. The Yb-nitrate hydrate used in this study contained an average of $3.3H_2O$ molecules per Yb atom as determined from ther-

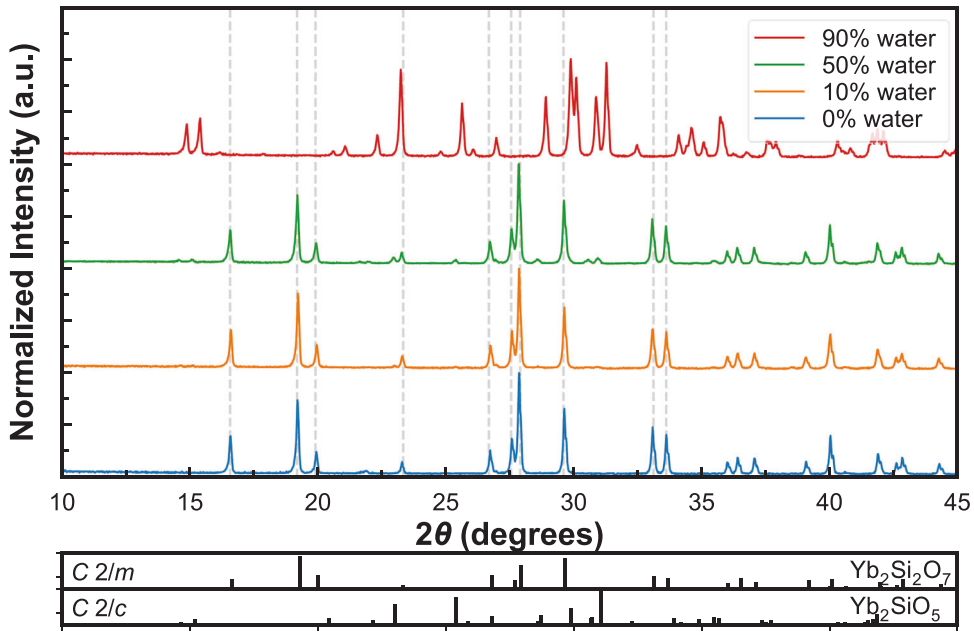

FIGURE 2 X-ray diffraction (XRD) patterns of Yb silicate sol–gels made with varying water contents with a pH of 2. The dashed vertical lines correspond to the *C* 2/*m* $Yb_2Si_2O_7$ phase. The degree of phase purity increases as water content decreases, with 90% water content being predominantly the Yb_2SiO_5 phase.

TABLE 1 Weight percentages of the *C* 2/*m* monoclinic phase in crystallized $Yb_2Si_2O_7$ sol–gels.

Yb disilicate weight fraction				
pH	**0% H_2O**	**10% H_2O**	**50% H_2O**	**90% H_2O**
2	100%	98.7% (1.3% MS)	94.4% (5.6% MS)	10% (85.7% MS)
Unaltered	88.4% (11.6% MS)	98.7% (1.3% MS)	~0% (81.3% MS)	~0% (61.3% MS)
10	97.5% (2.5% MS)	96.7% (3.3% MS)	75.6% (24.4% MS)	25.3% (74.7% MS)

Note: Values in parentheses indicate the weight percentage of Yb_2SiO_5 monosilicate phase. In cases where the total does not equal 100%, the balance is completed by ytterbium oxide. The "Unaltered" row indicates that only solvent and the RE and Si precursors were added to solution, but no acid or base was added to adjust pH.

mogravimetric analysis. This corresponds to $3.3H_2O$ per silicon atom in solution as Yb and Si were mixed in a 1:1 ratio. Typical relative humidity levels in the laboratory were 48.4% for a typical temperature 21.7°C. Additionally, the hydrolysis reaction of TEOS has been reported to be catalyzed by acids and bases, leading to the hypothesis that the final phase purity is controlled by the hydrolysis reaction of TEOS and not the rare-earth nitrate.[28,35–37] The catalysis of the hydrolysis reaction due to an acid or base is attributed to nucleophilic substitution reactions. There are many differing proposed exact reactions or mechanisms for both the acidic and basic regimes.[28,29,36,37]

Following the results of the Yb sol–gel experiments, the behavior of other individual rare-earth silicates was assessed, starting with Er. Observing phase formation for different rare earths under the same pH and water content conditions allowed a test of the hypothesis that the TEOS hydrolysis reaction is the rate limiting or controlling factor. Additionally, this knowledge of the pH and water dependence of phase formation was required for the eventual synthesis of a multicomponent ceramic that would utilize multiple rare-earth nitrates in solution to all react with TEOS. The XRD patterns for erbium disilicate are provided in Figures S3 and S4. Table 2 shows the weight percentages of the disilicate *C* 2/*m* phase in the 1400°C crystallized erbium silicate sol–gels. Similar to the ytterbium silicates, conditions of low water content and low pH result in greater phase purity. Only $Er_2Si_2O_7$ was observed for no intentional water additions and a pH of 2, which is the same behavior as observed for $Yb_2Si_2O_7$. The trend differs, however, from Yb in the pH = 10 series. In this case, the highest fractions of disilicate were observed for the 10 and 50% H_2O conditions rather than the no intentional water condition. The mechanisms driving this are

TABLE 2 Weight percentages of the *C* 2/*m* monoclinic phase in crystallized $Er_2Si_2O_7$ sol–gels.

Er disilicate weight fraction				
pH	**0% H_2O**	**10% H_2O**	**50% H_2O**	**90% H_2O**
2	100%	98.7% (1.3% MS)	94.4% (5.6% MS)	84.5% (15.5% MS)
10	88.0% (12.0% MS)	97.2% (2.8% MS)	93.8% (6.2% MS)	19.6% (80.4% MS)

Note: Values in parentheses indicate the weight percentage of monosilicate phase. In cases where the total does not equal 100%, the balance is completed by erbium oxide.

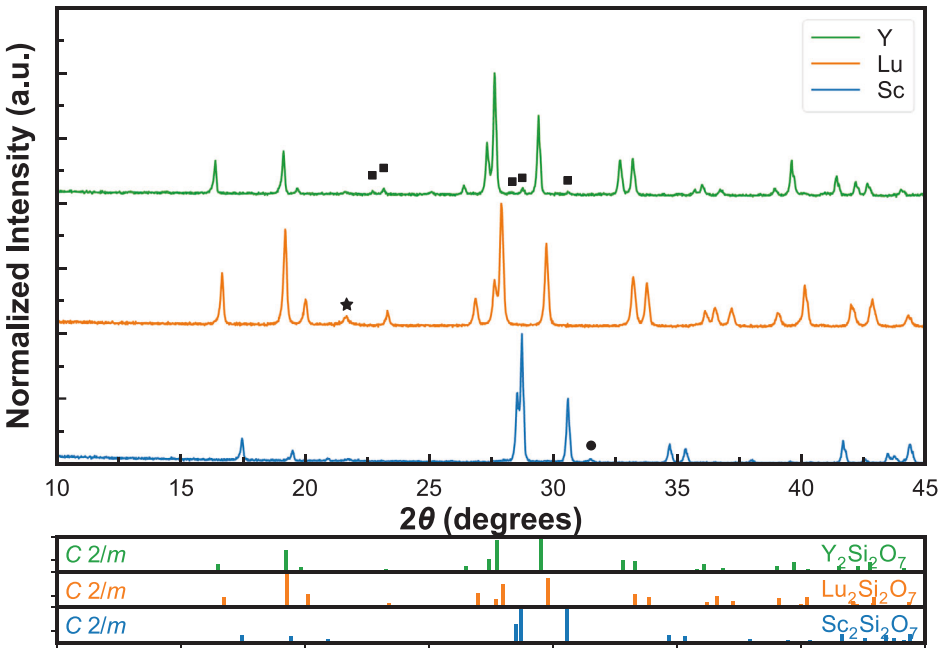

FIGURE 3 X-ray diffraction (XRD) patterns of Sc, Lu, and Y silicate sol–gels made with 0% water added and a pH of 2. All three are predominantly the *C* 2/*m* phase but do have secondary phases indicated by black squares, stars, and circles for the monosilicates, silica, and oxide phases, respectively.

unclear as the Er-nitrate was found to have $5.0H_2O$ per Er, which is higher than the Yb nitrate. Given this initial water content, it may have been expected that the 0% water condition should have behaved similar to the 10% and 50% conditions.

Regardless of the differences between Yb and Er silicate sol–gels at the high pH conditions, the maximum phase purity is again observed for a 0% intentional water addition and a pH of 2, suggesting that the Er nitrate provides sufficient water to drive the hydrolysis reaction of TEOS under acidic conditions. The water content of the other nitrates used was determined to be as follows: Lu-nitrate had approximately $3.6H_2O$, Sc-nitrate had approximately $9.5H_2O$, and Y-nitrate had approximately $6.0H_2O$. The trends in Yb and Er disilicate sol–gel synthesis were then tested for the Sc, Lu, and Y cations, replicating the 0% added water and target pH of 2. The XRD patterns of the 1400°C crystallized powders are shown in Figure 3. Some differences were noted in the final phase purity of the REDS relative to the Yb and Er sol–gels. Yttrium had a MS secondary phase, lutetium had a silica (cristobalite) secondary phase, and scandium had a scandium oxide secondary phase. More specifically, the disilicate phase in the Y sol–gel was 95.0 wt.%, with a 5.0% weight fraction of the MS phase. The Sc sol–gel had a disilicate weight fraction of 97.8% and a 2.2% weight fraction of a secondary scandium oxide phase.

The selection of Sc, Lu, Yb, Er, and Y for study as single-cation REDS provided the basis for the mixing of all five cations in equimolar concentrations to produce a multicomponent REDS under the same synthesis conditions. These five cations can crystallize in the *C* 2/*m* phase as single-cation REDS, with high or complete phase purity. Yttrium disilicate is known to have multiple polymorphs that are dependent on temperature,[16] but under the specific steps outlined in this work as a single component, Y disilicate stabilizes in the *C* 2/*m* phase. The next steps were to determine if the same procedure remained valid for producing phase-pure multicomponent REDS. Once again, the parameters of 0% water added and a pH of 2 were used

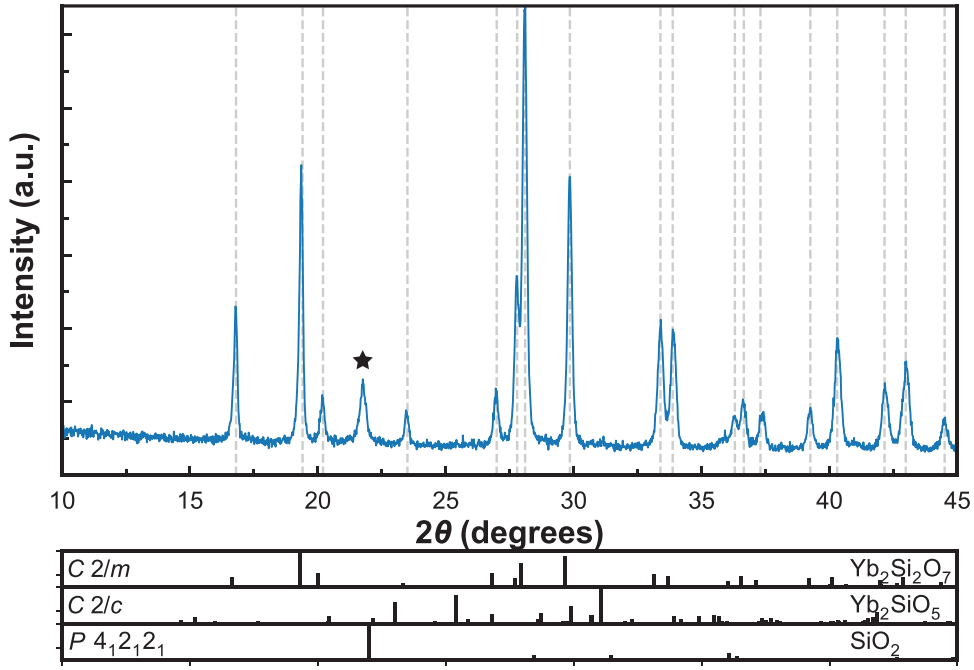

FIGURE 4 X-ray diffraction (XRD) pattern of a five component rare-earth disilicate (REDS). The *C* 2/*m* phase has been indexed via vertical dashed lines. The XRD pattern shows no secondary monosilicate phase and a silica peak at approximately 22° in 2θ, marked by a star symbol.

to produce a gel that was crystallized by heating to 1400°C and characterized via XRD. Figure 4 shows the pattern of $(Sc_{0.2}Lu_{0.2}Yb_{0.2}Er_{0.2}Y_{0.2})_2Si_2O_7$ with the disilicate *C* 2/*m* peaks indexed via vertical gray dashed lines. The multicomponent REDS produced shows phase purity similar to Yb and Er sol–gel-derived powders, where no MS or oxide phases are observed as secondary phases. There is a peak corresponding to cristobalite that appears at around 22° in 2θ. This indicates that the rare-earth nitrates most likely absorbed water prior to the synthesis procedure, resulting in their molecular weights to differ, causing the RE:Si ratio to deviate from 1:1 and the starting solution to be silica-rich. Regardless of the presence of silica, the synthesis procedures outlined here with an 18 h 1400°C thermal treatment illustrate the effect of water content and pH on the reaction rate of TEOS, with lower water concentration and low pH being ideal. Excessive amounts of water likely drive the TEOS hydrolysis to occur too quickly and result in SiO_2 segregating leading to MS formation. Importantly, this low water, low pH process is shown to produce many single and a multicomponent REDS with near phase purity.

3.2 | Crystallization and phase evolution of xerogel

Yb disilicate is widely reported to be stable in the *C* 2/*m* monoclinic phase, but prior work by Zhao et al. identified a lower temperature triclinic phase before the REDS crystallized into the monoclinic phase.[30] Besides their work, the triclinic phase was observed in two works by Garcia et al.[38,39] The samples in these works were not derived from sol–gel processes but were prepared via an air-plasma sprayed process. As the triclinic phase has been observed in materials processed by vastly different approaches, it is supportive that its formation is intrinsic to the crystallization process for ytterbium disilicate. Seminal works and phase diagrams for these materials typically only show data above 1400°C.[27] To fill the knowledge gap of phase evolution and to determine if similar triclinic phases form in other REDS, in situ hot stage XRD was used to observe the crystallization and potential phase transformations of sol–gel derived REDS. The following samples were characterized during heating in situ with XRD: $Yb_2Si_2O_7$, $Er_2Si_2O_7$, $Y_2Si_2O_7$, $Sc_2Si_2O_7$, and $(Sc_{0.2}Lu_{0.2}Yb_{0.2}Er_{0.2}Y_{0.2})_2Si_2O_7$. The synthesis methods described above that produced a single-phase REDS for each rare earth were utilized to produce xerogels that were then heat treated at 550°C and ground into fine powders for the in situ heating XRD experiments. Figure 5 shows the XRD patterns of a Yb sol–gel ramped from room temperature to 1200°C in a hot-stage XRD. The monoclinic peaks corresponding to the *C* 2/*m* phase are indexed with vertical dashed lines to illustrate phase presence.[32,33,40–42] The patterns show the initial crystallization of a triclinic phase that occurs between 950 and 1000°C. The triclinic phase transitions into the *C* 2/*m* phase as temperature increases. The in situ study is limited by the instrument's maximum

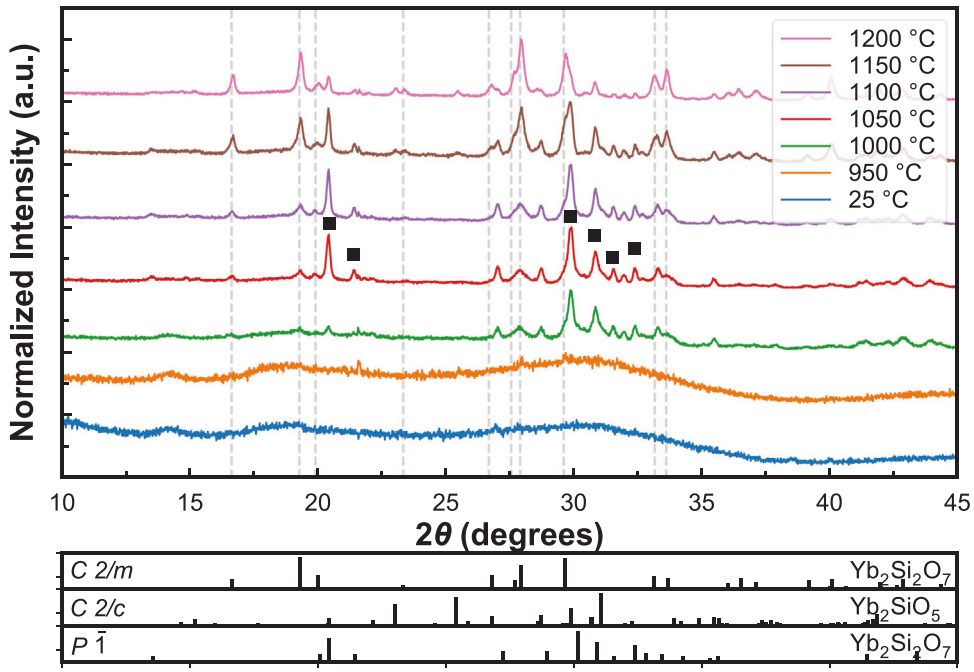

FIGURE 5 Diffraction patterns of in situ hot-stage X-ray diffraction (XRD) for a Yb silicate sol–gel. A triclinic phase nucleates at 1000°C and is eventually replaced by the *C* 2/*m* monosilicate phase. The triclinic phase is indexed above the 1050°C pattern by black squares.

temperature of 1200°C, but the ex situ experiments shown previously for the same sol–gel indicates that phase purity is also dependent on heat treatment temperature and time.

Subsequent REDS diffraction patterns are shown in Figures 6–9, showing intermediary phase compositions throughout the heating profile that differ from the ex situ work for each of Er, Y, and Lu disilicates, respectively. Er and Y XRD patterns in Figures 6 and 7, respectively, show the same triclinic to monoclinic phase transition as Yb, which is expected as these phases have been reported by Felsche.[16] Although the triclinic phase is prevalent during crystallization, it does not appear in the ex situ patterns of Yb, Er, and Y that were heat treated at 1400°C. The temperature of the triclinic to monoclinic disilicate phase transition is expected to increase with larger RE ionic radius as given by the phase boundaries described in Felsche's work.[16] This increase in crystallization temperature is noticeable during the heating in Figures 5 and 6, where the triclinic ytterbium disilicate phase crystallizes at a lower temperature than for erbium disilicate. The heat treatment temperature of the REDS holds great importance as do the synthesis parameters discussed in the previous sections. Given the maximum temperature limitations of the hot-stage, the in situ work could not reach the temperatures possible in the ex situ experiments, but it is hypothesized that the weight fraction of the monoclinic disilicate phase increases with temperature and time at temperature. The XRD patterns for Sc and Lu sol–gels shown in Figures 8 and 9, respectively, do not have the same polymorph transition from the triclinic to the monoclinic phase. Instead, the Lu sol–gel only has the MS and monoclinic disilicate phases. The weight fraction of the MS phase decreases as temperature increases, which matches the ex situ results shown previously in Figure 3 where Lu disilicate is the only phase. A similar trend is seen in the Sc sol–gel where instead of a triclinic phase or even the MS phase, there are two phases: the disilicate and scandium oxide. The Sc oxide weight fraction is prevalent at lower temperatures but begins to disappear with rising temperatures, again matching Figure 3.

The XRD patterns of $(Sc_{0.2}Lu_{0.2}Yb_{0.2}Er_{0.2}Y_{0.2})_2Si_2O_7$, a multicomponent REDS, during crystallization, are shown in Figure 10. The presence of the disilicate, *C* 2/*m* phase, is indicated by the vertical gray dashed lines. As illustrated, the *C* 2/*m* phase is the predominant phase in the crystalline material. Secondary phases, such as the triclinic phase of the disilicate as well as the MS, are present during crystallization that do not appear in ex situ XRD of the same material in Figure 4. The presence of the triclinic phase is small but is most evident when inspecting the broad peak shape at approximately 30° in 2θ that is rounded due to the presence of both the triclinic and monoclinic phases. As temperature increases, this peak sharpens as the triclinic phase fraction decreases. At above 20° in 2θ, a peak corresponding to the triclinic phase can also be seen at 1050°C. This peak decreases in intensity, indicating

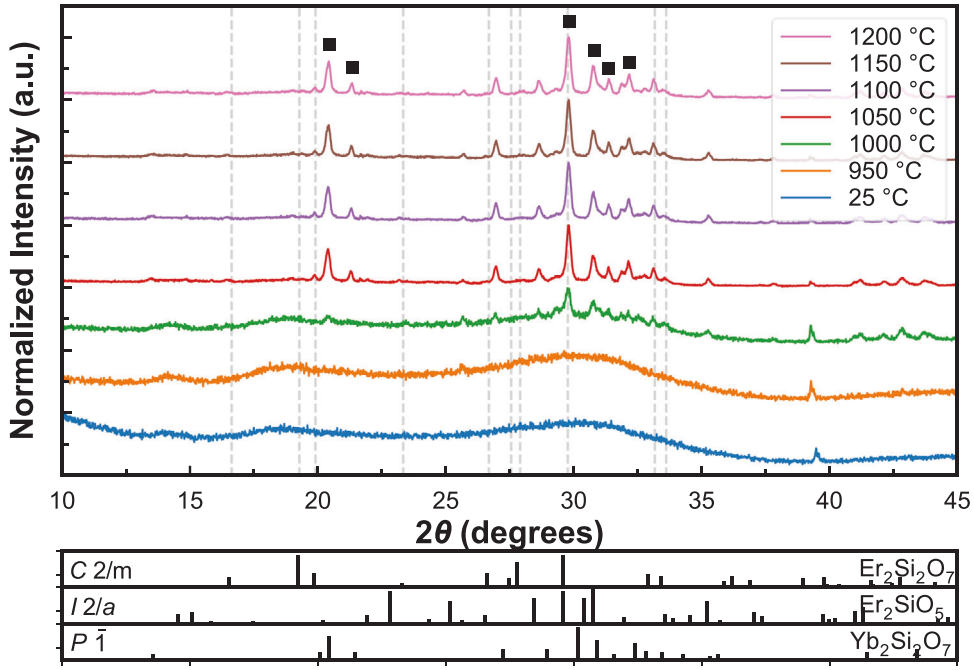

FIGURE 6 Hot-stage X-ray diffraction (XRD) of Er silicate sol–gel. The vertical dashed lines correspond to the *C* 2/*m* phase that is seen ex situ and is absent in the given patterns. The predominant polymorph is the triclinic phase where the pattern for the triclinic $P\bar{1}$ phase of Yb disilicate is given as a reference for general peak location in black below the plot and with black squares above the 1200°C pattern.

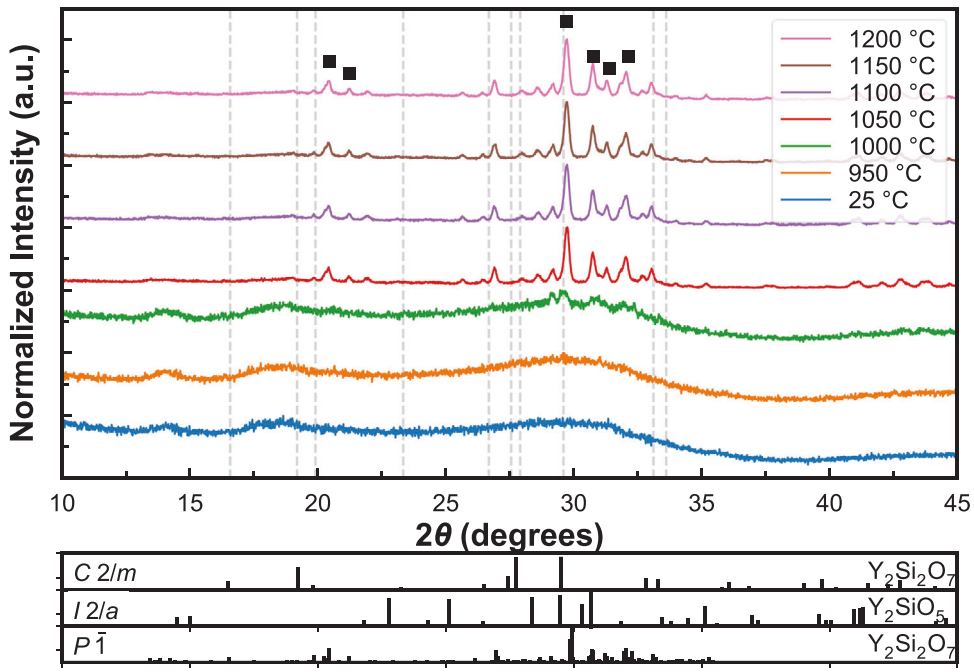

FIGURE 7 Hot-stage X-ray diffraction (XRD) of a Y silicate sol–gel. The vertical dashed lines correspond to the *C* 2/*m* phase that is seen ex situ and is absent in the given patterns. The peaks corresponding to the triclinic phase have been indexed by black squares above the 1200°C pattern.

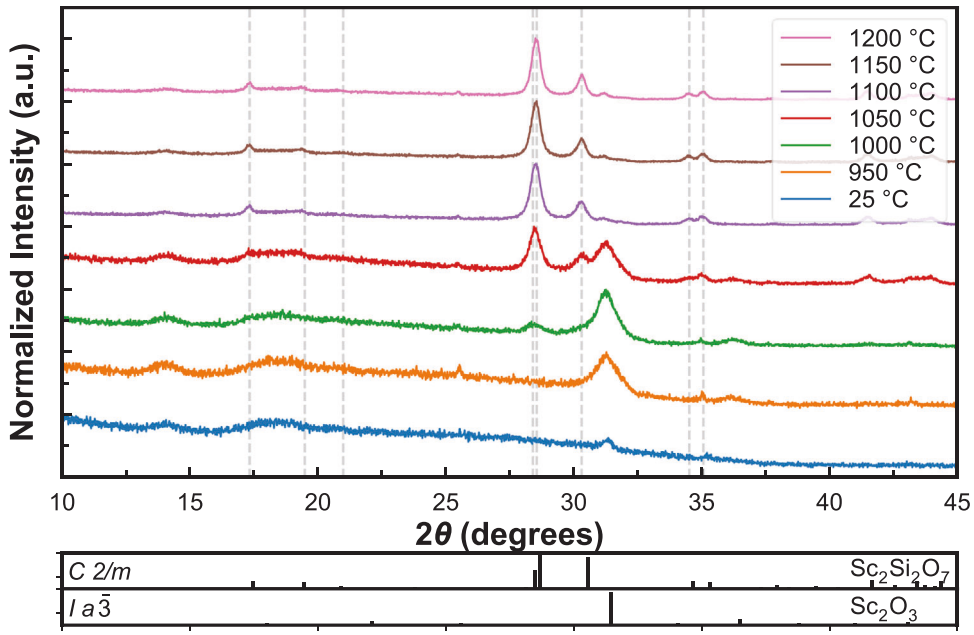

FIGURE 8 Hot-stage X-ray diffraction (XRD) of a Sc silicate sol–gel. The vertical dashed lines correspond to the $C\,2/m$ phase seen ex-situ. No triclinic or monosilicate was detected during crystallization. Instead, scandium oxide nucleates and decreases in weight fraction as temperature rises.

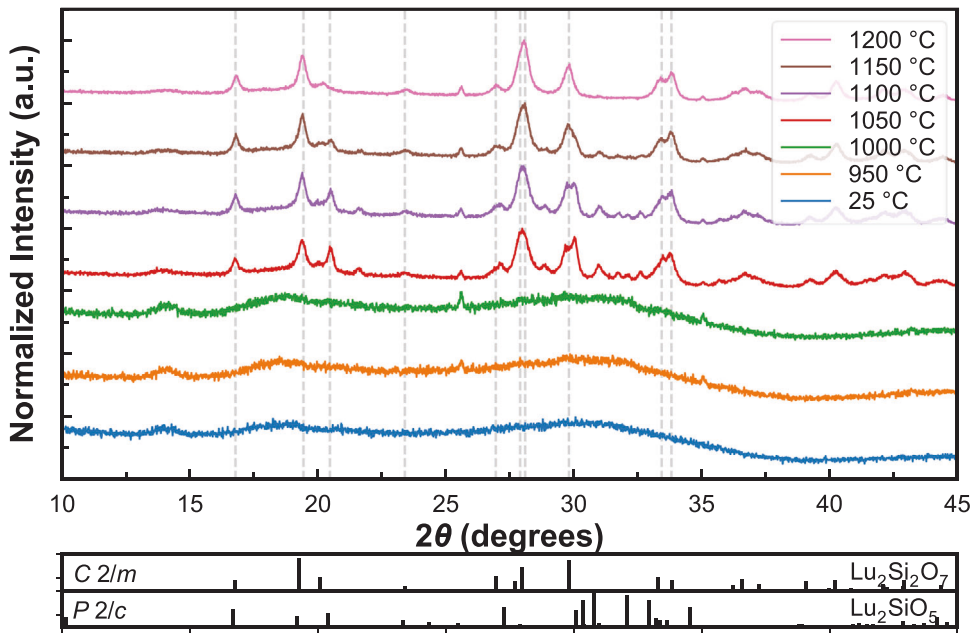

FIGURE 9 Hot-stage X-ray diffraction (XRD) of a Lu silicate sol–gel. The vertical dashed lines correspond to the $C\,2/m$ phase that was seen in ex situ experiments. A monosilicate phase is visible and decreases in weight fraction as temperature increases.

again the phase transformation. The presence of alumina is visible in the peaks at approximately 26° and 36° in 2θ, originating from the alumina sample holder. These results indicate the importance of high heat treatment temperatures and long heat treatment times to enable the complete evolution of the disilicate phase to produce a phase-pure final material.

To gain insight into the progression of the triclinic to monoclinic phase transformation during crystallization, additional ex situ crystallization studies were performed

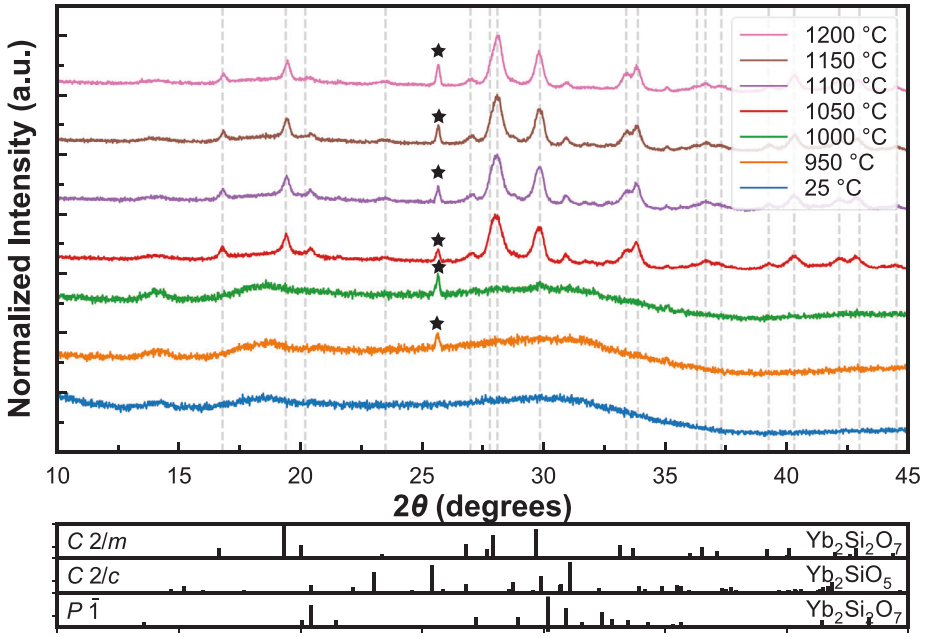

FIGURE 10 In situ X-ray diffraction (XRD) of the multicomponent rare-earth disilicate (REDS) with the following composition: $(Sc, Lu, Yb, Er, Y)_2Si_2O_7$. Reference patterns for Yb disilicate polymorphs and Yb monosilicate are given below, and vertical dashed lines indicate the approximate location of $C\,2/m$ peaks. A star is used to mark an alumina sample holder peak.

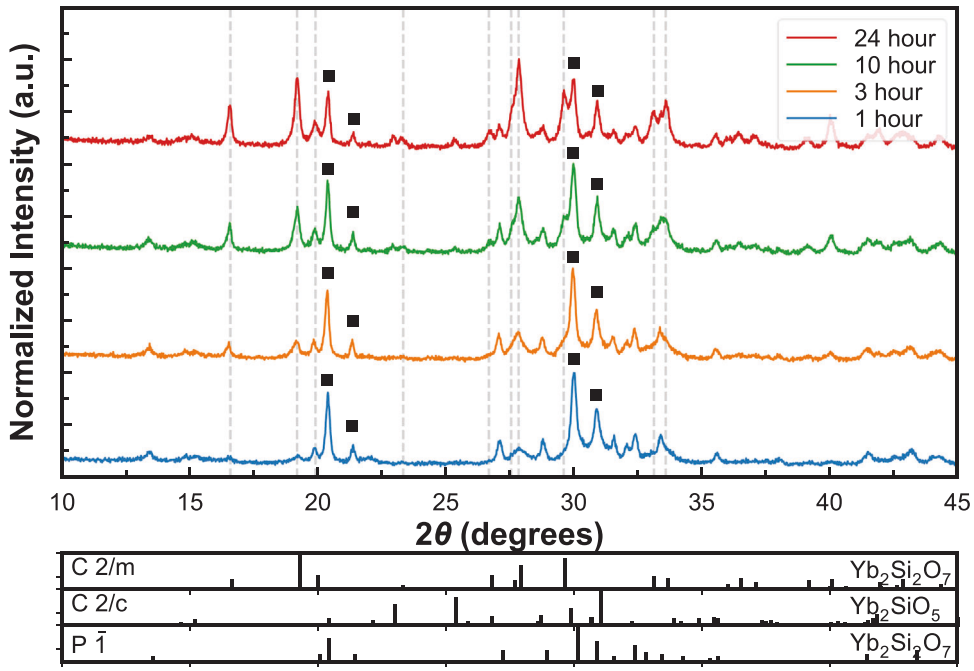

FIGURE 11 X-ray diffraction (XRD) patterns for Yb disilicate sol–gel derived powders heat treated at 1000°C for 1, 3, 10, and 24 h. The dashed vertical line indicates the peak positions of the monoclinic disilicate phase. The black squares indicate the triclinic peaks.

on the Yb disilicate. Figure 11 shows the ex situ crystallization of Yb disilicate sol–gels at four different heat treatment durations at 1000°C. The vertical dashed lines indicate the locations of the monoclinic disilicate phase. The triclinic phase nucleates first and eventually converts into the monoclinic phase as time and temperature increase. The weight fractions of the triclinic phase for the 1, 3, 10, and 24-h heat treatments are 96.9%, 91.5%, 62.4%,

and 46.0%, repectively, suggesting a slow transformation from the triclinic to monoclinic phase. The most intense monoclinic disilicate peak, at approximately 28° in 2θ as seen in Figure 4, results in a broad peak shape in the lowest heat treatment times. The peak sharpens as heat treatment time increases and indicates the contrast in nucleation and growth behavior of the monoclinic and triclinic phases. The broad peaks are due to small crystallites that then grow at longer time and temperature.

The triclinic phase may present a design challenge for implementation of REDS as T/EBCs due to the phase transition from triclinic to monoclinic with initial heating. This phase transformation could potentially be deleterious because of thermomechanical instability of the coating. To illustrate this potential challenge, the unit cell volumes of the triclinic and monoclinic structures of the disilicates were normalized by the formula units (f.u.) per unit cell volume. The molar volume of monoclinic $Er_2Si_2O_7$ phase being 143.65 $Å^3$/f.u. and the triclinic $Er_2Si_2O_7$ phase is only 130.08 $Å^3$/f.u., suggesting an expansion of 10.4% upon transforming from the triclinic to the monoclinic phase.[16] Garcia et al. reported the molar volumes of the two polymorphs of $Yb_2Si_2O_7$ as 78.29 and 85.52 cm^3 for the triclinic and monoclinic phase, respectively. The transformation into the monoclinic phase results in a 9.24% volume expansion.[39] This substantial difference will lead to thermal expansion stresses as the phase transformation occurs with a large expansion between the triclinic and monoclinic phases.

4 | CONCLUSION

This work outlines conditions that can be used to prepare REDS powders with high phase purity. The use of little to no water, low pH, and high heat treatment temperatures resulted in higher phase purity for the desired disilicate phase for single cation and multicomponent REDS. The synthesis of single cation and multicomponent REDS via sol–gel requires control of the TEOS hydrolysis reaction to produce an intended final-phase mixture. Too fast of hydrolysis driven by excess water likely leads to the segregation of SiO_2, which prevents the atomic scale mixing necessary to realize $RE_2Si_2O_7$ as the first crystallization product. The use of in situ and ex situ XRD to study crystallization showed the importance of processing temperature and phase evolution that occurs as the temperature is increased. An intermediate triclinic phase seen in the crystallization of Yb, Er, and Y disilicates has been confirmed and can be a potential hazard to thermomechanical stability within a REDS T/EBC. Several other REDS had secondary phases (MS, silica, and oxide) appear and subsequently disappear during crystallization, and the origin of these phases likely was related to water content and/or nonstoichiometric batching due to water adsorbed on the rare-earth nitrate precursors. Understanding the sol–gel processing criteria and crystallization behavior allows production of more consistent phase-pure REDS, informs the synthesis of producing mixed-phase powders with desired ratios, and outlines the amorphous to crystalline transition that REDS may see as T/EBCs in application.

ACKNOWLEDGMENTS

This work was supported by the U.S. National Science Foundation's (NSF) Designing Materials to Revolution and Engineer our Future (DMREF) program under award number 1921973. Utilization of the Panalytical Empyrean, X'pert, and Anton Parr Hot-Stage instruments within UVA's Nanoscale Materials Characterization Facility (NMCF) was fundamental to this work.

ORCID

Alejandro Salanova https://orcid.org/0000-0001-7799-8612

Elizabeth J. Opila https://orcid.org/0000-0001-5540-7084

Jon F. Ihlefeld https://orcid.org/0000-0003-0166-8136

REFERENCES

1. Padture NP. Advanced structural ceramics in aerospace propulsion. Nat Mater. 2016;15(8):804–9. https://doi.org/10.1038/nmat4687
2. Padture NP. Environmental degradation of high-temperature protective coatings for ceramic-matrix composites in gas-turbine engines. npj Mater Degrad. 2019;3(1):11. https://doi.org/10.1038/s41529-019-0075-4
3. Lee KN, Fox DS, Bansal NP. Rare earth silicate environmental barrier coatings for SiC/SiC composites and Si3N4 ceramics. J Eur Ceram Soc. 2005;25(10):1705–15. https://doi.org/10.1016/j.jeurceramsoc.2004.12.013
4. Spitsberg I, Steibel J. Thermal and environmental barrier coatings for SiC/SiC CMCs in aircraft engine applications. Int J Appl Ceram Technol. 2004;1(4):291–301.
5. Lee KN, Fox DS, Eldridge JI, Zhu D, Robinson RC, Bansal N, et al. Upper temperature limit of environmental barrier coatings based on mullite and BSAS. J Am Ceram Soc. 2003;86(8):1299–306. https://doi.org/10.1111/j.1151-2916.2003.tb03466.x
6. Opila EJ, Smialek JL, Robinson RC, Fox DS, Jacobson NS. SiC recession caused by SiO_2 scale volatility under combustion conditions: II, thermodynamics and gaseous-diffusion model. J Am Ceram Soc. 1999;82(7):1826–34.
7. Robertson AL, Solá F, Zhu D, Salem J, White KW, Microscale fracture mechanisms of HfO_2-Si environmental barrier coatings. J Eur Ceram Soc. 2019;39(7):2409–18. https://doi.org/10.1016/j.jeurceramsoc.2019.02.001
8. Harder BJ. Oxidation performance of Si-HfO_2 environmental barrier coating bond coats deposited via plasma spray-physical vapor deposition. Surf Coat Technol. 2020;384:125311. https://doi.org/10.1016/j.surfcoat.2019.125311

9. Anton R, Leisner V, Watermeyer P, Engstler M, Schulz U. Hafnia-doped silicon bond coats manufactured by PVD for SiC/SiC CMCs. Acta Mater. 2020;183:471–83. https://doi.org/10.1016/j.actamat.2019.10.050
10. Xu Y, Hu X, Xu F, Li K. Rare earth silicate environmental barrier coatings: present status and prospective. Ceram Int. 2017;43(8):5847–55. https://doi.org/10.1016/j.ceramint.2017.01.153
11. Cao XQ, Vassen R, Stoever D. Ceramic materials for thermal barrier coatings. J Eur Ceram Soc. 2004;24(1):1–10. https://doi.org/10.1016/S0955-2219(03)00129-8
12. Braun JL, Rost CM, Lim M, Giri A, Olson DH, Kotsonis GN, et al. Charge-induced disorder controls the thermal conductivity of entropy-stabilized oxides. Adv Mater. 2018;30(51):1805004.
13. Ridley M, Gaskins J, Hopkins P, Opila E. Tailoring thermal properties of multi-component rare earth monosilicates. Acta Mater. 2020;195:698–707.
14. Salanova A, Brummel IA, Yakovenko AA, Opila EJ, Ihlefeld JF. Phase stability and tensorial thermal expansion properties of single to high-entropy rare-earth disilicates. J Am Ceram Soc. 2023;106(5):3228–38. https://doi.org/10.1111/jace.18986
15. Kotsonis GN, Almishal SSI, Marques dos Santos Vieira F, Crespi VH, Dabo I, Rost CM, et al. High-entropy oxides: harnessing crystalline disorder for emergent functionality. J Am Ceram Soc. 2023;106(10):5587–611. https://doi.org/10.1111/jace.19252
16. Felsche J. Polymorphism and crystal data of the rare-earth disilicates of type $RE_2Si_2O_7$. J Less-Common Met. 1970;21(1):1–14.
17. Shannon RD. Revised effective ionic radii and systematic studies of interatomic distances in halides and chalcogenides. Acta Crystallogr A. 1976;32(5):751–67.
18. Boakye EE, Mogilevsky P, Hay RS, Cinibulk MK. Rare-earth disilicates as oxidation-resistant fiber coatings for silicon carbide ceramic-matrix composites: oxide, oxidation resistant coating for SiC/SiC composite. J Am Ceram Soc. 2011;4(6):1716–24. https://doi.org/10.1111/j.1551-2916.2010.04306.x
19. Li Y, You B, Zhao W, Zhang W, Yin M. Synthesis and luminescent properties of nano-scale $Y_2Si_2O_7:Re^{3+}$ (Re = Eu, Tb) phosphors via sol-gel method. Chin J Chem Phys. 2008;21(4):376–80. https://doi.org/10.1088/1674-0068/21/04/376-380
20. Parmentier J, Bodart PR, Audoin L, Massouras G, Thompson DP, Harris RK, et al. Phase transformations in gel-derived and mixed-powder-derived yttrium disilicate, $Y_2Si_2O_7$, by X-ray diffraction and 29Si MAS NMR. J Solid State Chem. 2000;149(1):16–20. https://doi.org/10.1006/jssc.1999.8474
21. Boonstra AH, Bernards TNM. The dependence of the gelation time on the hydrolysis time in a two-step SiO_2 sol-gel process. J Non-Cryst Solids. 1988;105(3):207–13.
22. Hench LL, West JK. The sol-gel process. Chem Rev. 1990;90(1):33–72. https://doi.org/10.1021/cr00099a003
23. Jayaseelan DD, Ueno S, Ohji T, Kanzaki S. Sol–gel synthesis and coating of nanocrystalline Lu2Si2O7 on Si3N4 substrate. Mater Chem Phys. 2004;84(1):192–95.
24. Hreniak D, Strek W, Opalińska A, Nyk M, Wołcyrz M, Lojkowski W, et al. Luminescence properties of Tb-doped yttrium disilicate prepared by the sol–gel method. J Sol–Gel Sci Technol. 2004;32:195–200.
25. Jothinathan E, Vanmeensel K, Vleugels J, Van der Biest O. Powder synthesis, processing and characterization of lanthanum silicates for SOFC application. J Alloys Compd. 2010;495(2):552–55. https://doi.org/10.1016/j.jallcom.2009.10.106
26. Feldhoff A, Arnold M, Martynczuk J, Gesing TM, Wang H. The sol–gel synthesis of perovskites by an EDTA/citrate complexing method involves nanoscale solid state reactions. Solid State Sci. 2008;10(6):689–701. https://doi.org/10.1016/j.solidstatesciences.2007.11.030
27. Toropov NA, Bondar IA. Silicates of the rare earth elements. IV. New silicates in the lanthanum oxide–silica system. Izv Akad Nauk SSSR Ser Khim. 1961;5:739–44.
28. Brinker CJ, Scherer GW. Sol-gel science: the physics and chemistry of sol-gel processing. Cambridge, MA: Academic Press; 2013.
29. Brinker CJ. Hydrolysis and condensation of silicates: effects on structure. J Non-Cryst Solids. 1988;100(1–3):31–50. https://doi.org/10.1016/0022-3093(88)90005-1
30. Zhao C, Wang F, Sun Y, Zhou Y. Synthesis and characterization of β-$Yb_2Si_2O_7$ powders. Ceram Int. 2013;39(5):5805–11. https://doi.org/10.1016/j.ceramint.2013.01.001
31. Toby BH, Von Dreele RB. GSAS-II: the genesis of a modern open-source all purpose crystallography software package. J Appl Crystallogr. 2013;46(2):544–49. https://doi.org/10.1107/S0021889813003531
32. Smolin YI, Shepelev YF. The crystal structures of the rare earth pyrosilicates. Acta Crystallogr B. 1970;26(5):484–92.
33. Smolin YI. Crystal structure of ytterbium oxyorthosilicate Yb_2SiO_5. Sov Phys Crystallogr USSR. 1970;14(6):854.
34. Saiki A, Ishizawa N, Mizutani N, Kato M. Structural change of C-rare earth sesquioxides of Yb_2O_3 and Er_2O_3 as a function of temperature. J Ceram Soc Jpn. 1985;93(10):649–54.
35. Rahaman MN. Ceramic processing. Boca Raton, FL: CRC Press; 2017. https://doi.org/10.1201/9781315157160
36. Voronkov MG, Yuzhelevskii YA, Mileshkevich VP. The siloxane bond and its influence on the structure and physical properties of organosilicon compounds. Russ Chem Rev. 1975;44(4):355.
37. McNeil KJ, DiCaprio JA, Walsh DA, Pratt RF. Kinetics and mechanism of hydrolysis of a silicate triester, tris(2-methoxyethoxy)phenylsilane. J Am Chem Soc. 1980;102(6):1859–65. https://doi.org/10.1021/ja00526a015
38. Garcia E, Sotelo-Mazon O, Poblano-Salas CA, Trapaga G, Sampath S. Characterization of $Yb_2Si_2O_7$–Yb_2SiO_5 composite environmental barrier coatings resultant from in situ plasma spray processing. Ceram Int. 2020;46(13):21328–35. https://doi.org/10.1016/j.ceramint.2020.05.228
39. Garcia E, Garces HF, Turcer LR, Bale H, Padture NP, Sampath S. Crystallization behavior of air-plasma-sprayed ytterbium-silicate-based environmental barrier coatings. J Eur Ceram Soc. 2021;41(6):3696–705. https://doi.org/10.1016/j.jeurceramsoc.2020.12.051
40. Müller-Bunz H, Schleid T. Über die Oxidsilicate M_2O [SiO_4] der schweren Lanthanoide (M = Dy–Lu) im A-Typ. Z Für Anorg Allg Chem. 1999;625(4):613–18.
41. Soetebier F, Urland W. Crystal structure of lutetium disilicate, $Lu_2Si_2O_7$. Z Für Krist-New Cryst Struct. 2002;217:22–22.
42. Smolin YI, Shepelev YF, Titov AP. Refinement of crystal-structure of thortveitite $Sc_2Si_2O_7$. Kristallografiya. 1972;17(4):857–58.

SUPPORTING INFORMATION

Additional supporting information can be found online in the Supporting Information section at the end of this article.

How to cite this article: Salanova A, Opila EJ, Ihlefeld JF. Phase purity and evolution in sol–gel derived single component and multicomponent rare-earth disilicates. J Am Ceram Soc. 2024;107:3687–700.
https://doi.org/10.1111/jace.19672